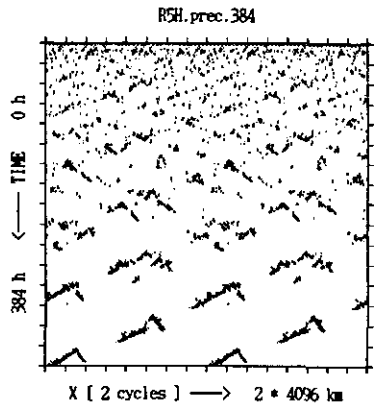

Figure 1: Time evolution of rainfall distribution in case HC. Two cycles of 4,096 km domain is shown from left to right. Time goes down from 0 h to 384 h.

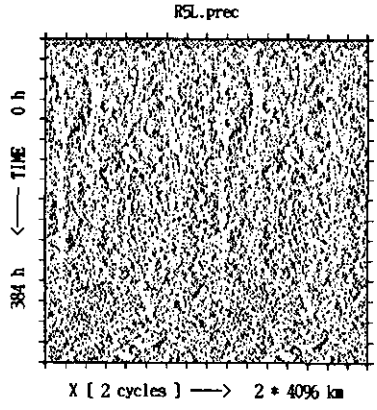

Figure 2: Same as Fig.1 but for case LC.

tensity for the case HC. At first, precipitation occurs almost randomly. As time goes on, cloud activity becomes organized into propagating wavy pattern. In the end, almost all rainfall is concentrated in two wave number one structures that run in the opposite direction; because their amplitude is almost the same, we can regard it as a standing oscillation. On the other hand, rainfall distribution for the case LC, shown in Fig.2, lacks significant large scale modulation from the beginning to the end of the experiment.

The vertical distributions of latent heating realized in the two experiment (not shown here) reflected that of the specified body coolings; i.e., it was enhanced in higher levels for case HC, whereas it was enhanced in the lower levels for case LC. This is consistent with the prediction of the linear wave-CISK theories that points upper-enhanced cumulus heating as necessary factor for amplifying propagating disturbance. The spatial structure (not shown) and the phase velocity can be interpreted in the framework of linear wave-CISK theories.

b. dependence of preffered scale on surface wind speed

The case HC above gives only the lower limit of preferred scale of wave-CISK disturbances. So in order to identify the preffered scale, case HC was repeated using the 16,384 km domain model whose result is shown in Fig.3, which shows that the preffered wavelength does exsist and is about 4000km. It should be noted that this is much shorter than the preffered scale of WISHE (longer than 16000 km as shown in Nakajima,1993,1994).

The preffered wavelength was found to be sensitive to V_{sfc}, the specified wind speed in the bulk formulae used for the surface flux calculations. Fig.4 shows the result of the case where V_{sfc} = 1m/s, and Fig.5 shows that of the case with V_{sfc} = 30m/s. (I note here that V_{sfc}=3m/s in the standard cases.) Comparing Fig.3-5, we see that wavelength is longer in the case with smaller V_{sfc}, whose reason remains unclear. One possibility is that the wavelength is proportional to the period of wave that must match the PBL recovery time, which will probably be long if Vscf is smaller.

c. Failure of linear wave-CISK theories

Closely examining Fig.5 again, we notice an wave number one stationaly amplifying modulation. This type of stationaly structure becomes more evident when we further increase V_{sfc} (not shown). If one want to explain the coexsitence of propagating and statinaly modes in the linear wave-CISK theory, one must assume different proportional coefficient on cumulus heating and large scale vertical motion in propagating and stationaly modes. This exemplifies one of the limitations of linear theory, which may be useful as a framework of interpretion but can not be very useful for prediction.

Another example of the limitations of wave-CISK theory is its 'failure' in predicting the preffered scale. 'Positive-only' wave-CISK gives better prediction (growth rate flattens in the limit of long wave), but it is not sufficient. However, we must note that the prediction on the growth rate itself is not bad. In fact, even in case HC where wave number one dominates, patterns of much shorter wavelength are evident in the earlier time; i.e., shorter wave do grow faster but do not grow into very large amplitude. The same success and failure applies in the WISHE case; linear theory successfully predicts faster growth of shorter waves, but one will get false infirmation if he or she expects those waves to be dominant in the longer timescale. This type of pitfall is, in retrospect, common to usual flow instability theories.

5.Concldíng remarks

We could simulate wave-CISK type disturbances in WISHE-free surface flux condition. The phase velocity, spatial structure, and the dependence on the cloud heating parameter are consistent with the prediction of linear wave-CISK theories. Realized scale selection in terms of the finally attained wavelength is, however, significantly different from that given by the growth rate-wavelength relationship in the linear theories.

Combined with WISHE results, the wave-CISK experiments offers useful example of explicitly simulated cumulus-LS interaction. Because the real

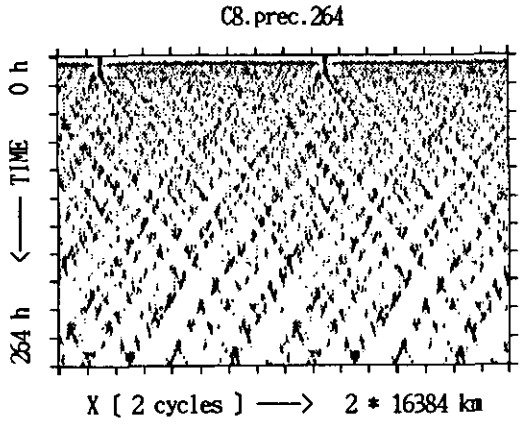

Figure 3: Time evolution of rainfall distribution in case HC in large model. Two cycles of 16,384 km domain is shown from left to roght. Time goes down from 0 h to 264 h.

observation suffers from severe undersampling, this type of study will be very important for improvement of our quantitative and qualitative understandings on the role of cumulous convection in the atmosphere. Of course the limitation that comes from the model's 2-dimensional geometry should be checked, but it must be left for studies in future, which may not be near considering the required tremendous computational resources.

Acknowledgements

Computations are done by SX-3 at NIES. The author very much thanks to the staff members of NIES, especially Dr.Numaguti, for the technical help in usage of the SX-3 system.

References

1. Nakajima, K. (1994): Direct simulation of large scale organizations of cumulus convection. Ph.D Dissertation at University of Tokyo. 144p. (in Japanese. English version will be available from author.)

2. Nakajima, K. (1993): Ultra-high resolution modeling of the tropical atmosphere. CGER'S SUPERCOMPUTER ACTIVITY REPORT 1992., pp.8-9.

3. Yamasaki,M. (1969): Large-scale disturbances in the conditionally unstable atmosphere in low latitudes. Pap.Meteor.Geophys., 20, 289-336.

4. Hayashi,Y. (1970): A theory of large-scale equatorial waves generated by condensation heat and accelerating the zonal wind. J.Meteor.Soc.Japan, 48,140-160.

5. Lindzen,R. (1974): Wave-CISK in the tropics. J.Atmos.Sci.,31,156-179.

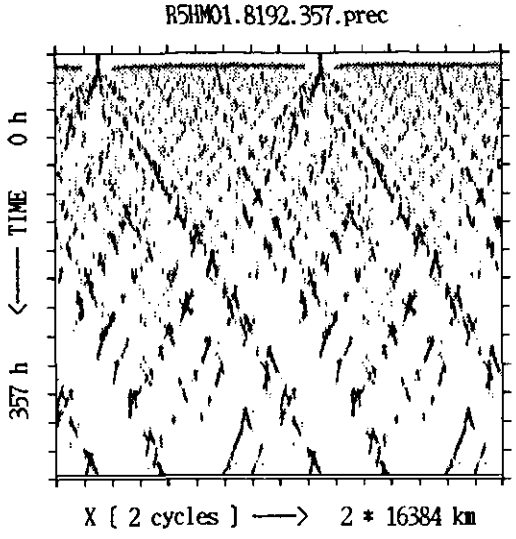

Figure 4: Same as Fig.3 but for the case with V_{sfc} = 1 m/s. Time goes down from 0 h to 357 h.

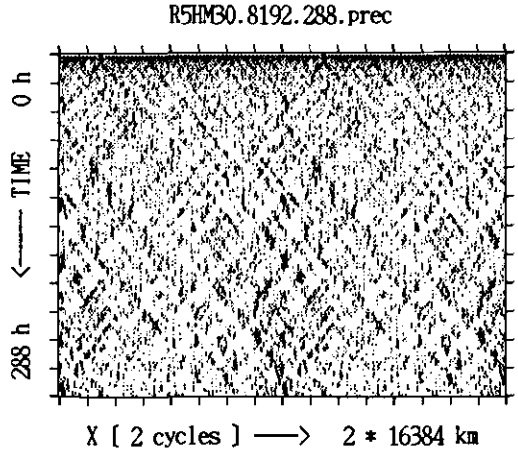

Figure 5: Same as Fig.3 but for the case with V_{sfc} = 30 m/s. Time goes down from 0 h to 288 h.

Development of an Atmospheric General Circulation Model for Climate Research

Contact Person	Atusi Numaguti Atmospheric Environment Division, National Institute for Environmental Studies, Japan Environmental Agency.
Research Organization	Seiji Sugata, Shigeki Mitsumoto National Institute for Environmental Studies Masaaki Takahashi, Toshiro Kumakura, Teruyuki Nakajima, Akimasa Sumi, Taroh Matsuno Center for Climate System Research, University of Tokyo.

Keywords climate model, atmosphere, parameterization, radiation, land surface, clouds

1 Background

A quantitative evaluation of climate change such as the global warming is impossible without a high-quality numerical model which describes the dynamics of the climate system and the circulations of the energy and material. The purpose of this research is to develop a community climate model which enables research into mechanism of the climate change with the time scales ranging from several years to hundreds of years.

At the present time, there are about five comprehensive atmosphere-ocean combined climate models in the world. Also, the atmospheric general circulation models are developed at about ten organizations and are used for the experiment of carbon dioxide doubling. These models give qualitatively similar results for the global warming prediction, but do not coincide quantitatively with one another. For example, the global average of the temperature rise at CO_2 doubling varies from 2°C to 5°C depending on the models. In addition, the ability of each model in reproducing the current climate is not satisfactory. For example, the ocean-atmosphere coupled models cannot yield realistic climate maps without making an artificial adjustment of the flux between atmosphere and ocean. These problems are attributed to the incomplete representation of physical processes and limited spatial resolution.

Under these circumstances, this project of the development of a climate model and improvement of the representation of physical processes is started toward the quantitative estimation of the climate change.

2 Objective

The goal of our research is the quantitative estimation of the climatic change using a comprehensive climate model of atmosphere-ocean-land climate system. Currently, we are developing a atmospheric part of the model, *i.e.*, an atmospheric general circulation model (AGCM).

The basic standpoint in the development is to make the model based on obvious physics and possibly less dependent on empirical parameters. Effective model code was employed to make the long-term run possible with high resolution. In addition, considerable attention was paid to the readability and module compatibility of the code to enable a community use of the model.

The model is based on a simple AGCM developed at University of Tokyo [1]. In order to make the model suitable for climate research, developments on the following three points are required. The first is the improvement of the parameterization of physical processes. Particularly, the parameterizations of radiative transfer, cloud precess, and land-surface processes are very important. The second is the preparation of dataset for use of the model as boundary condition. The third is the testing on the model ability for reproducing the current climate and the tuning of the model parameters, the parameterization schemes, and the boundary conditions.

3 Model Description

The outline of the current model is summarized as the followings.

Basic Equations: 3-dimensional hydrostatic primitive equations on sphere with normalized pressure (σ) coordinate.

Prognostic Variables: Horizontal velocity, temperature, surface pressure, total water content, soil temperature, soil moisture, snow depth.

Discretezation: Spectral transformation method with Gaussian grid in horizontal and an grid differentiation [2] in vertical. Leap-frog scheme is used for time integration.

Resolution: Variable, currently tested with T42 (2.8° grid) 20 levels and T21 (5.6° grid) 20 levels.

Physical Processes: k-distribution model for radiative transfer [3].
Arakawa-Schubert [4] type cumulus parameterization with prognostic closure.
Estimation of cloud liquid water by prognostics

of the total water content [5].
Mellor-Yamada [6] level 2 turbulence scheme.
Simple non-local diffusion scheme.
Bulk scheme for surface fluxes [7].
Multi-layer treatment of land-surface energy budget and hydrology [8].
Gravity-wave drag scheme [9].

4 Results

4.1 Seasonal Climatology Experiment

Introducing physical parameterizations reported above, the model was run under realistic boundary conditions for long times (about 10 year) and the results were compared with observed climatology fields. The adopted horizontal resolutions is T21(equivalent grid size 5.5°) or T42(3°) and vertical resolution is 20 levels.

The zonally averaged distribution of temperature of T21 run and its deviation from observed climatology is shown in Fig.1 for three month average from June to August. The deviation is less than two degrees in most part of the troposphere. However, there is large cold bias near the tropopause region, especially near the pole.

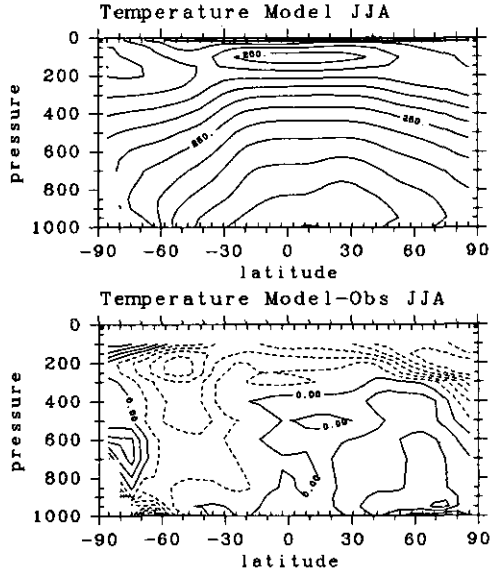

Fig.1 Distribution of zonal mean temperature (upper) and its deviation from observed climatology (lower). Three month average from June to August is shown. Contour interval is 10K(upper) and 2K(lower).

The distribution of precipitation is shown in Fig.2. The location and strength of the large-scale precipitation area is well simulated.

By examining the model result, it is found that the model reproduces fairly realistic climate except for some problems, for example, too dry tropical middle troposphere and too moist upper troposphere (Fig.3) and small precipitation in Amazon region in austral summer.

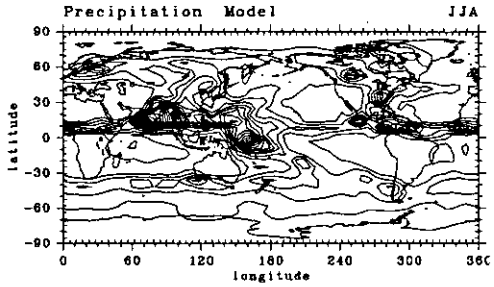

Fig.2 Distribution of precipitation. Three month average from June to August is shown. Contour interval is 50mm/month.

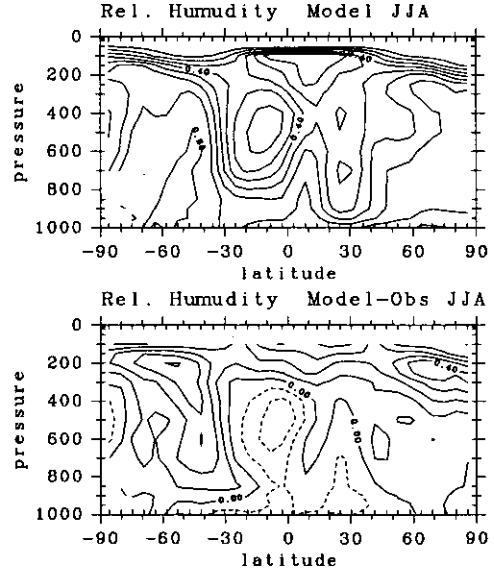

Fig.3 Distribution of zonal mean relative humidity (upper) and its deviation from observed climatology (lower). Three month average from June to August is shown. Contour interval is 10%.

4.2 Development of parameterization schemes

Development of efficient radiation code: In order to solve the transfer equation efficiently, the Discrete Ordinate/Adding method is adopted in our scheme. However, the number of channels of absorption that the model computes is extremely limited even with the scheme. We have overcome this difficulty by adopting k-distribution method and by applying a nonlinear optimization scheme for the selecting the channels. As the result, we can reduce the number up to 48 from 242 keeping the error of the heating rate to be smaller than 0.5 ° K/day below 40 km altitude [3].

Cloud liquid water content prediction: In order to express the feedback process concerning the cloud

optical thickness appropriately, an scheme for the prediction of cloud liquid water content is developed. In this scheme, the predicting variable is the total water content. The liquid water is diagnosed assuming the variability of the total water within the grid. The precipitation and evaporation of rain is estimated by simplified Kessler type formula. It is confirmed the scheme successfully reproduce the observed long and short radiative fluxes at the top of the atmosphere.

Modified Arakawa-Schubert cumulus parameterization: An Arakawa-Schubert type cumulus parameterization is developed. The mass flux is prognostically estimated using cloud work function. The effect of downdraft is incorporated in a rather simple manner.

Improved treatment of boundary layer processes: The effect of cloud is incorporated in the vertical diffusion process by use of moist Richardson number. In the surface flux parameterization, the effect of free convective motion is incorporated to improve the evaporation field over the tropical ocean. The effect of non-local diffusion in the boundary layer is also incorporated.

Sensitivity study with soil model: Aiming to the development of comprehensive land surface model in use of climate model, a simple sensitivity study are done using an one-dimensional model of land surface [8]. A one-dimensional soil model with explicit treatment of ground water table was developed. The model is based on thermal diffusion equation and Richards' equation for soil water. The model was coupled with a simple model of atmospheric boundary layer and was run for long time with various conditions of precipitation and radiation as external forcing. The result indicates the importance of appropriate treatment of the deep water and runoff in the long-term behavior of the land surface.

Incorporation of vegetation effect: An attempt in incorporating the effect of vegetation into the land surface model is done basically following the SiB model [10]. Results of one dimensional simulation with and without the effect of transpiration and interception show significant difference in the seasonal pattern of evaporation.

5 Summary

An atmospheric general circulation model for use of the climate study is developed and tested in the ability reproducing the present climate. The result is generally good, except for some problems probably due to inadequateness of physical parameterization. The improvement of the parameterization schemes, particularly for the cloud-radiation interaction and land surface processes is required. Also, more comprehensive test of the model performance not only for the averaged climate but also for the variability is needed for the validation and further improvement of the model.

6 Acknowledgments

This research is supported by Global Environment Research Program of Japan Environmental Agency. Assistance by Dr. A. Abe-Ouchi, Messrs. M. Tsukamoto, S. Emori, and T. Nishimura is greatly appreciated.

References

1. A. Numaguti, *J. Atmos. Sci.*, **50**, 1874–1877 (1993)
2. A. Arakawa A. and M.J. Suarez, *Mon. Weather Rev.*, **111**, 34–45 (1983)
3. T. Nakajima and M. Tsukamoto, *in preparation* (1994)
4. A. Arakawa and W.H. Schubert, *J. Atmos. Sci.*,, **31**, 671–701 (1974)
5. H. Le Treut and Z.-X. Li, *Climate Dynamics*, **5**, 175–187 (1991)
6. G.L. Mellor and T. Yamada, *J. Atmos. Sci.*, **31**, 1791–1806 (1974)
7. J. Louis, *Bound. Layer Meteor.*, **17**, 187–202 (1979)
8. S. Mitsumoto, S. Emori and K. Abe, *J. Japan Soc. Hydrol. Water Res.* , **7**, 259–267 (1994)
9. N.A. McFarlane, *J. Atmos. Sci.*, **44**, 1775-1800 (1987)
10. P.J. Sellers, Y. Mintz, Y.C. Sud, A. Dalcher, *J. Atmos. Sci.*, **43**, 305–331 (1986)

A role of Hadley circulations and baroclinic waves in the global angular momentum budget

Contact Person Masaki Satoh
Department of Mechanical Engineering, Saitama Institute of Technology
Okabe, Saitama, 369-02, Japan

Keywords Hadley circulation, baroclinic waves, axisymmetric model, angular momentum budget

1. Introduction

Observationally, it is well known that the Hadley cells in the low-latitudes and the Ferrel cells as a zonal average of baroclinic waves in mid-latitudes play important roles in the angular momentum budgets of the general circulation [1]. Theoretical understandings of the Hadley circulations are promoted by using axisymmetric models [2,3]. It is not sufficiently known, however, to what extent these symmetric circulations describe more realistic asymmetric ones. Williams [4,5] has compared axisymmetric circulations with asymmetric ones by using a general circulation model (GCM). However, it is difficult to extract general conclusions from his results, since he used the "swamp" condition as the surface boundary condition [6]. It is the aim of this study to calculate symmetric and asymmetric circulations with GCM under the prescribed surface temperature distribution, so as to investigate roles of the Hadley and Ferrel cells in the angular momentum budgets, particularly through dependencies on the rotation rates.

2. Model

The GCM developed at the University of Tokyo [7] is used to calculate asymmetric and axisymmetric states (here after, 3D and 2D, respectively). The resolution of 3D is T42 and 16 layers. In 2D, the modes of wave number zero alone are used in longitudinal direction. The moist adjustment scheme, a simple non-gray radiation model, and the level II of Yamada and Meller boundary layer schemes are used as physical processes. The surface temperature is prescribed as $300\mathrm{K} - 40\mathrm{K} \times \sin^2\varphi$ (φ is latitude), and the surface is assumed to be wet (an aqua planet model). Integrations are started from a state at rest with a uniform temperature 250K. An equilibrium state of 3D is defined by a mean of 80 – 160 days, whereas one of 2D by a mean of 200 – 400 days. Dependencies on rotation rates Ω are examined: $\Omega/\Omega_0 = 3$, 1 and 1/3, where Ω_0 is the rotation rate of the earth.

3. Results

Figs. 1 (a)–(c) show meridional distributions of zonal winds for 2D. At the equator, zonal winds are easterly from the surface to the upper troposphere, while in the mid- and high-latitudes they are westerly except for the bottom layers. The width of the equatorial easterly are smaller as Ω is larger. Easterlies develop in the low-latitudes where direct cells (the Hadley cells) exist. In the mid- and high-latitudes, a multiple cellar structure (symmetric cells) exists. The moving symmetric cells will no longer exist in 3D; the Richardson number of the averaged state of the mid-latitudes is approximately 10, so that it is in a baroclinic unstable regime [8].

Figs. 1 (d)–(f) show meridional distributions of longitudinal mean zonal winds for 3D. At the equator, there are easterlies in the lower layers, while westerlies in the upper troposphere. These westerlies are not so strong that they form a jet (a maximum of westerly). In the mid-latitudes, westerlies prevail from the top to the bottom layers. Because of the existence of baroclinic waves, angular momentums are effectively transported downward in comparison to 2D. The surface winds near the poles are easterlies for $\Omega/\Omega_0 \geq 1$, where polar direct cells exist.

4. Discussion and further comments

The mass fluxes of the Hadley circulation of 3D, Ψ_H, can be approximately expressed in terms of the external parameters by using the simple Hadley models of 2D [3,6], although they are more or less larger than those of 2D,

The mass fluxes of the Ferrel cells in 3D, Ψ_F,

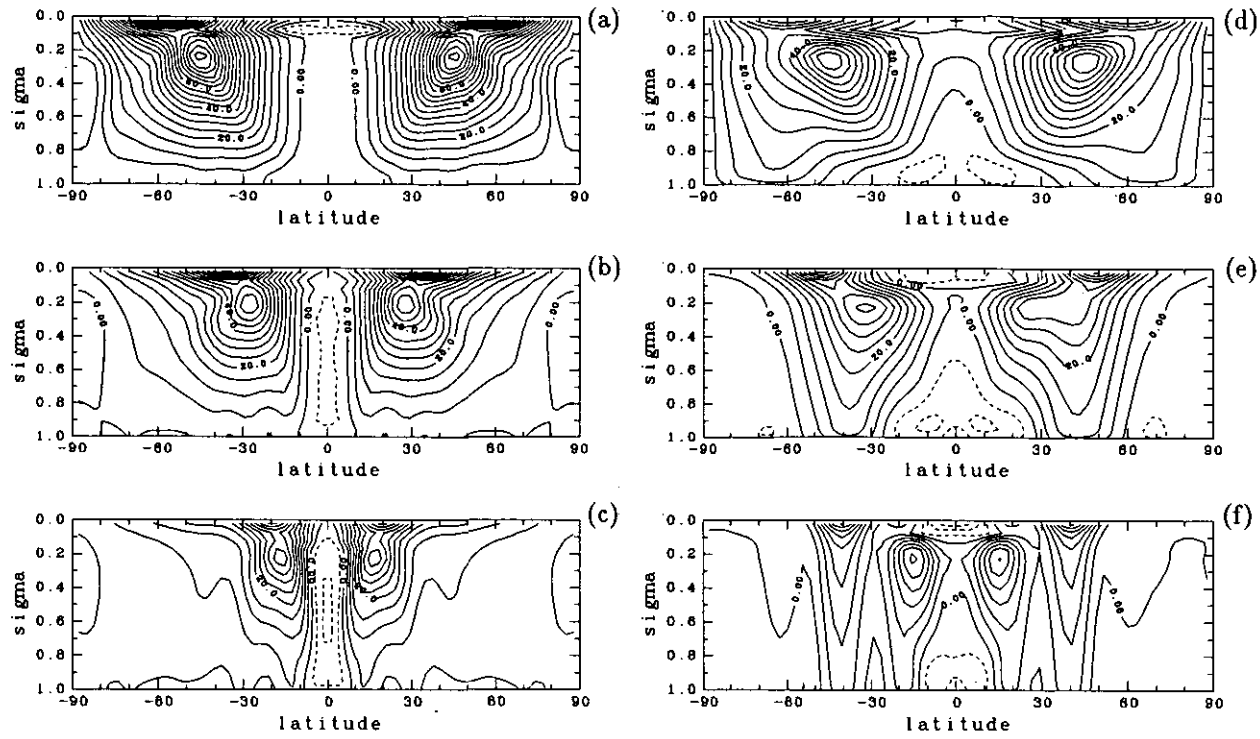

Fig. 1. Meridional distributions of zonal winds for (a) 2D, $\Omega/\Omega_0 = 1/3$, (b) 2D, $\Omega/\Omega_0 = 1$, (c) 2D, $\Omega/\Omega_0 = 3$, (d) 3D, $\Omega/\Omega_0 = 1/3$, (e) 3D, $\Omega/\Omega_0 = 1$, and (f) 3D, $\Omega/\Omega_0 = 3$. Contour intervals are 5 m/s.

are related with those of the Hadley cells through the angular momentum budgets. The upward transports of the angular momentum in the Hadley cells are balanced by the downward ones in the Ferrel cells, so that one may have

$$\frac{\Psi_F}{\Psi_H} = -\frac{\Delta l_H}{\Delta l_F} = -\frac{\Delta\varphi_H}{2\Delta\varphi_F} \approx -\frac{1}{2}, \qquad (1)$$

where Δl_H, Δl_F are differences of the angular momentums between the upward and downward branches in the the respective cells. Their absolute components are related with the latitudinal widths of the cells, $\Delta\varphi_H$, $\Delta\varphi_F$, where $\Delta\varphi_H \approx \Delta\varphi_F$ can be assumed as in Eq. (1).

One may also discuss the relations between the Hadley cells and the amplitudes of the baroclinic waves and the latitudinal energy transports by the baroclinic waves by using theories of baroclinic instability. This picture will give another point of view for the life cycle of cyclones and the estimation of heat transport in energy budget models.

Acknowledgments

Figures were produced by GFD-DENNOU libraries and GTOOL3 by Dr. Numaguti.

References

1. E. Palmen and W. Newton, *Atmospheric Circulation Systems*, Academic Press, 603pp (1969)
2. E. K. Schneider, *J. Atmos. Sci.*, **34**, 280-296 (1977)
3. I. M. Held and A. Y. Hou, *J. Atmos. Sci.*, **37**, 515-533 (1980)
4. G. P. Williams, *Climate Dynamics*, **2**, 205-260 (1988)
5. G. P. Williams, *Climate Dynamics*, **3**, 45-84 (1988)
6. M. Satoh, *J.Atmos. Sci.*, **51**, 1947-1968 (1994)
7. A. Numaguti, *J. Atmos. Sci.*, **50**, 1874-1887 (1993)
8. P. H. Stone, *J. Atoms. Sci.*, **23**, 390-400 (1966)

The study of mass transport between the troposphere and stratosphere

Contact Person Isamu Yagai
Meteorological College, Meteorological Agency of Japan.

(Research Organization) Koji Yamazaki
Masaru Chiba
Kiyotaka Shibata
Tatsusi Tokioka
Akira Noda
Meteorological Research Institute

Key Words ozone, mass transport, the troposphere and stratosphere ,sea surface temperature, global warming

1. Backgrounds

Predicting climate change due to an increase in atmospheric carbon dioxide was first studied using simplified one-dimensional models such as radiative-convective models. These models, however, could not represent the horizontal transport of heat, water vapor, ozone and other substances. Therefore, the three-dimensional general circulation developed at the Meteorological research Institute (MRI) is used in this study to asses the influence of the global warming to the transport of ozone.

2. Objective

In order to simulate the current distribution of ozone well, we will make improvement of the MRI GCM. Furthermore, we will estimate the effect of global warming to the redistribution of ozone.

3. Method

The first is the perpetual July experiment by the 12 layer MRI GCM with the $\pm 2°C$ SST (Sea surface temperature) perturbations. This was time integrated for 90 days and the last 30 days were analyzed. The results with the global sensitivity and surface fluxes are presented by Cess et al. (1991)[1] and Randall et al. (1992)[2].

The second is the seasonal run by the 12 layer GCM which is started from the atmospheric condition at 12Z 15 December 1982. Stratospheric sudden warmings appear in the course of the experiment. The simulated zonal mean ozone mixing ratio are compared with the observation.

We have developed 15 layer version of the MRI GCM by increasing the vertical resolution in the troposphere. The 15 model levels are approximately 1.39, 2.68, 5.18, 10.0, 19.3, 37.3, 72.0,119, 168, 237, 335, 457, 589, 741, 912 hPa, while the 12 layer model has 5 levels in the troposphere corresponding approximately to 150, 300, 500, 700, and 900 hPa. The model was started from 00Z 1 January 1979 and time integrated for 3 years. The distribution of sea surface temperature is prescribed based on climatological data (Climate RUN). In addition we completed another experiment where the zonally uniform SST anomaly was added to the climatological value and the concentration of the carbon dioxide was doubled (Warming RUN).

4. Results

In the perpetual July experiment, the ozone in the stratosphere decreased while the ozone in the troposphere increased in the $+2°C$ SST perturbation experiment. This result is caused by dynamical effects since the zonally integrated photochemical ozone production rates tend to increase ozone in the stratosphere.

In the seasonal run by the 12 layer GCM, stratospheric sudden warmings appear in the course of the experiment. The simulated zonal mean ozone mixing ratio is compared with the observation. The maximum value and the height over the equator is almost coincide with the observation. Simulated ozone in the this experiment increases in the middle stratosphere while it decreases in the upper stratosphere due to the advective process during the sudden warmings.

Figure 1 shows the zonal mean ozone mixing ratio (ppm) in parts per million by mass for January by the 15 layer GCM. The maximum value and its height over the equator is almost coincide with the observation.

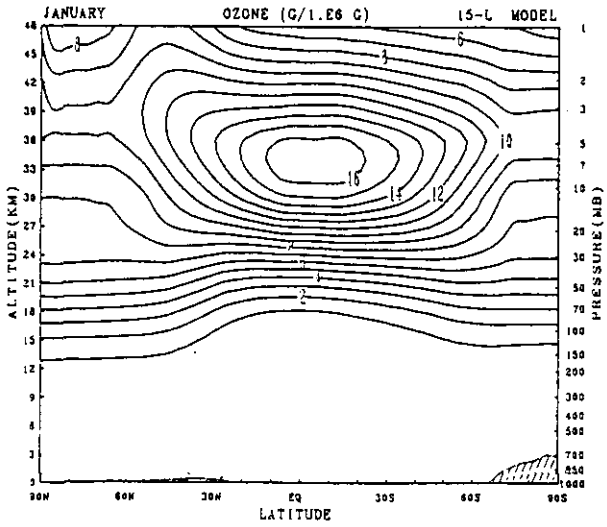

Figure 1: Zonally and monthly averaged ozone mixing ratio (ppm) by the 15 layer MRI GCM (Climate RUN).

Figure 2 shows the difference of ozone mixing ratio for January between Climate RUN and Warming RUN. Figure 3 is the same as figure 2 but for the ozone photochemical production rate. The ozone decreases in the upper stratosphere at polar night region, while the ozone increases around 60 °N in the upper stratosphere. The change of ozone in this region is caused by the dynamical process, while at lower latitudes in the stratosphere ozone increases by the photochemical process through the change of temperature in this region. These results, however, have to be checked in the analysis of longer period since the model as well as real atmosphere has considerable variation on interannual time scales.

Reference

Cess, R.D., G.L. Potter, M.-H . Zhang, J.P. Blanchet, S. Chalita, R. Coloman, D.A. Dazlich, , A.D. Del Genio, V. Dymnikov, V. Galin, D. Jerrett, E. Keup, A.A. Lacis, H.Le. Treut, Z.-X. Li, X.-Z. Liang, J. F. Mahfouf, B.J. McAvaney, V.P. Meleshko, J.F.B. Mitchell, J.-J. Morcrette, P. M. Norris, D.A. Randall, L. Rikus, E. Roeckner, J. F. Royer, U. Schlese, D.A. Sheinin, J.M. Slingo, A.P. Sokolov, K.E. Taylor, W.M. Washington, R.T. Wetherald, and I. Yagai, : Interpretation of snow-climate feedback as produced by 17 General Circulation Models. Science, 253, 888-892, 1991.

D.A. Randall, R.D. Cess, J.P. Blanchet, G.J. Boer, D.A. Dazlich, A.D. Del Genio, M. Déqué, V. Dymnikov, V. Galin, S.J. Ghan, A.A. Lacis, H.Le. Treut, Z.-X. Li, X.-Z. Liang, B.J. McAvaney, V.P. Meleshko, J.F.B. Mitchell, J.-J. Morcrette, G.L. Potter, L. Rikus, E. Roeckner, J.F. Royer, U. Schlese, D.A. Sheinin, J. Slingo, A.P. Sokolov, K.E. Taylor, W.M. Washington, R.T. Wetherald, I. Yagai, and M.-H . Zhang, : Intercomparison and Interpretation of surface energy fluxes in atmospheric general circulation models. J. Geophys. Res., 97, 3711-3724, 1992.

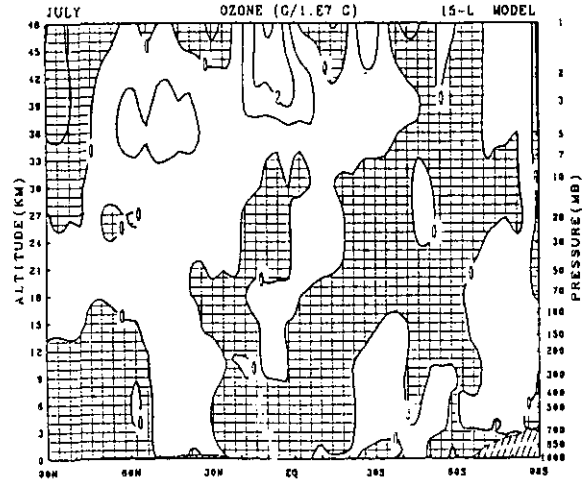

Figure 2: The difference of ozone mixing ratio (0.1 ppm) for January, Warming RUN-Climate RUN. Negative values are shaded.

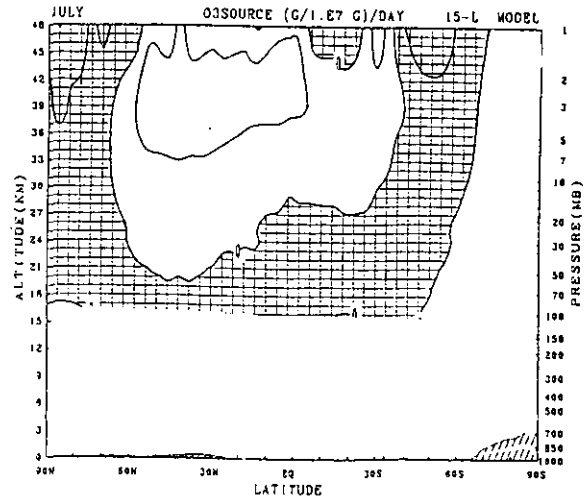

Figure 3: The difference of ozone photochemical production rate (0.01 ppm/day) for January, Warming RUN-Climate RUN. Negative values are shaded.

2. Atmospheric and Oceanic Environment Modeling

Study of Basin-Scale Ocean Circulation related to Global Chlorophyll Distribution

Contact Person: Laboratory head, Masahiro Endoh
Meteorological Research Institute,
Tsukuba, 305 Japan

(Research Organization): Yoshiteru Kitamura, Goro Yamanaka, Atsushi Obata, Tatsuo Motoi and Yoshifumi Nogi
Meteorological Research Institute

Keywords: global ocean circulation model, surface mixed layer, chlorophyll, satellite ocean color data

1. Background

Recently, effects of human activity are expanding to the global ocean scale. Necessity of evaluating anthropogenic effects is increasing. Satellite ocean color data is one of the most efficient indicators of ocean surface content of chlorophyll or phytoplankton as oceanic primary productivity, which is affected by the nutrient distribution sometime related to the environmental deterioration. Therefore we need to develop useful ocean satellite data set to evaluate the ocean environment.

2. Objective

For preparing useful ocean satellite chlorophyll data for evaluation of the ocean environment, it is necessary to realize the relationship between global chlorophyll distribution and global ocean circulation as a physical factor which affects the biochemical environment of the ocean.

As the first step, we develop a global ocean circulation model which resolves processes influencing the chlorophyll distribution, such as circulation in the surface layer, depth of the surface mixed layer, upwelling of deep water and so on. Next, we compare horizontal structure of the surface mixed layer reproduced by this model, with the global satellite-derived chlorophyll distribution.

3. Method

A numerical model employed is a standard global ocean circulation model with realistic bottom and coastal topography and resolution of 2.5° x 2° x 21 levels (Endoh et al. 1994(4)). Embedded in the model is a turbulent mixed layer model which has a closure scheme of level 2 (Mellor & Yamada, 1982(3)) with 5 meters resolution in the upper 20 meters. It gives a set of turbulent mixing coefficients of temperature/salinity and momentum, which actually mixes water in the vertical direction and predicts new temperature/salinity and current.

4. Results

In this study, the model is driven by the monthly mean climatological wind stress (Hellerman & Rosenstein, 1983(1)), monthly mean temperature and seasonal mean salinity (Levitus, 1982(2)) after equilibrium calculation with the annual mean climatology forcing as reported in (4). Using the CGER's Supercomputer, the calculation is carried out for 11 years until it reaches to a quasi-steady state with seasonal variation.

Fig.1 and Fig.2 indicate global distributions of the surface mixed layer depth in February (winter in the northern hemisphere) and in August (summer in the northern hemisphere) of the 11th model year, respectively. We defined the surface mixed layer depth as the depth where the downward temperature deviation in a vertical grid column reaches 0.5 °C measured from the sea surface.

Fig.1 (winter in the northern hemisphere) shows that deep mixed layers develop in the Kuroshio current region, Gulf Stream and extension regions of these western boundary currents, and also in the northern part of the Mediterranean Sea. These deep mixed layers are formed by strong vertical mixing due to cooling of the surface saline water. In other regions except the Antarctic Circumpolar Current, wind driven Ekman mixed layers are seen and these depths are about 40 meters in average. In the central area of the equatorial Pacific, surface mixed layer is deeper than the observed climatology. It may be caused by well known overestimation of easterly wind stress in the original Hellerman and Rosenstein's data set.

In the North Pacific, deep mixed layer occupies mainly western mid-latitudes. On the other hand, in the North Atlantic, deep mixed layer extends to the whole mid-latitudes. The difference is due to different eastward transports of saline water by the western boundary currents.

Wind driven Ekman mixed layer with the depth of about 40 meters extends over the whole North Pacific in summer (Fig.2). In the winter Antarctic Circumpolar Current, depth of the mixed layer exceeds 200 meters over the large region. Especially, mixed layers are deeper in the western boundary current (Agulhas, East Australian current and these extension) of the subtropical gyre in the southern hemisphere.

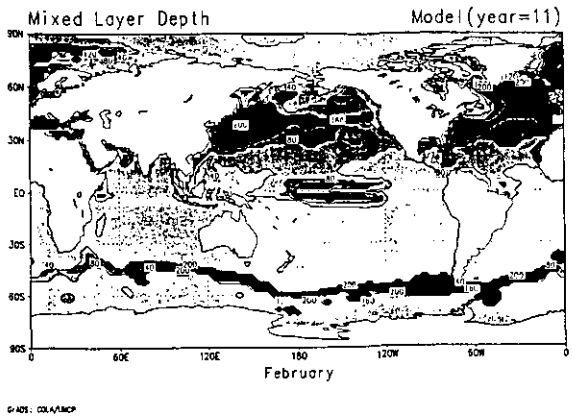

Fig.1 Distribution of the surface mixed layer depth in the model (February). Contours indicate 40, 80, 120, 160 and 200 m deep.

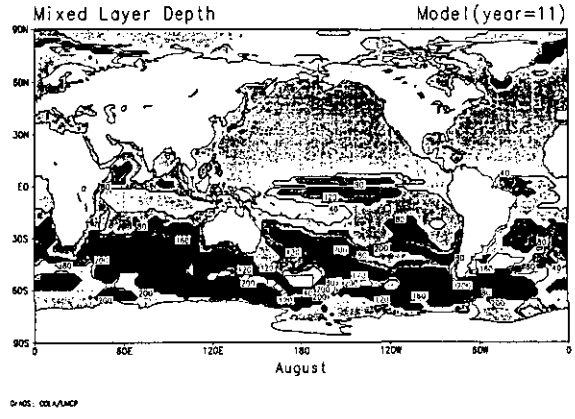

Fig.2 Distribution of the surface mixed layer depth in the model (August). Contours indicate 40, 80, 120, 160 and 200 m deep.

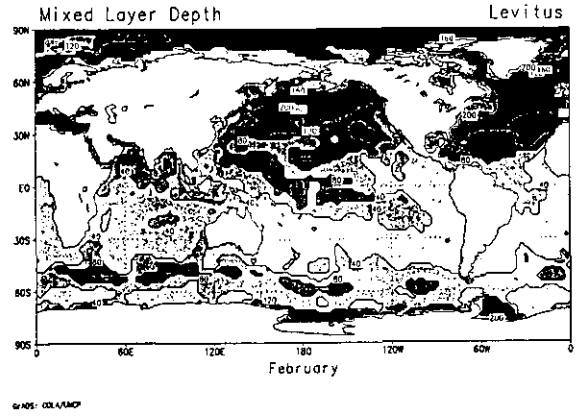

Fig.3 Distribution of the surface mixed layer depth (February) estimated from the Levitus climatology. Contours indicate 40, 80, 120, 160 and 200 m deep.

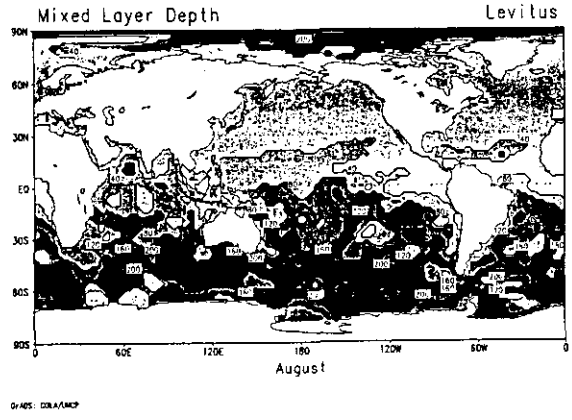

Fig.4 Distribution of the surface mixed layer depth (August) estimated from the Levitus climatology. Contours indicate 40, 80, 120, 160 and 200 m deep.

In Fig.3 and Fig.4, global distributions of the surface mixed layer depth in the Levitus climatology are shown in February and August, respectively. Comparing Fig.1 with Fig.3 (February), or Fig.2 with Fig.4 (August), model and climatology are similar to each other in terms of the basin-scale pattern of distributions of the surface mixed layer depth.

5. Summary

A global ocean circulation model with a turbulent closure mixed layer model is integrated for 11 years with climatological monthly mean forcing. In accordance with analysis of the in-situ observed temperature data, the global ocean circulation model well simulates that mixed layers for the winter convection season in the North Pacific are deepest in the western subarctic/subtropical region, while in the North Atlantic, deep mixed layers extend to the whole higher latitudes. In the Southern Oceans, basin-scale convective mixed layer is deepest along the Antarctic Circumpolar Current.

In the future study, spatial and seasonal variations of model surface mixed layer will be compared with those of global chlorophyll distribution derived from satellite ocean color data. Upgrade of the closure scheme in the mixed layer model from level 2 to level 2.5 is also planned.

References

1. S.Hellerman and M.Rosenstein, *J.Phys.Oceanogr.* 13,1093 (1983)
2. S.Levitus, *NOAA Prof.Papers* . 13,173pp.(1982)
3. G.L.Mellor and T.Yamada, *Rev.Geophys.Space Phys.* 20,851 (1982)
4. M.Endoh et al., CGER's Supercomputer Activity Report 1992,31 (1994)

Development of the Transport, Transformation and Removal model for Acidic and Oxidative Pollutants in the East Asia

Contact person

Junji Sato
Applied Meteorology Research Department
Meteorological Research Institute
Japan Meteorological Agency

(Research Organization)

Takehiko Satomura
Hidetaka Sasaki
Shunji Takahashi
Kikuo Okada

Keywords

Acid Rain, Long-range Transport, Numerical Model, Deposition, Transformation

1. Background and objective

Recently, more than 23 million ton/ year of SOx is released into the atmosphere over the East Asia, and it is to be feared that they are transported in long distance and acid deposition affects biosphere. In the East Asia, however, observation network of acid deposition is not developed. Therefore one has no method to estimate amount of acid deposition except using numerical model.

To understand transport process of atmospheric pollutants related with acid rain and to estimate amount of acid deposition , a long-range transport numerical model which has transformation and deposition of pollutants by precipitation is developed. Recent investigations reveal that in-cloud scavenging such as cloud nucleation of pollutants through the process of cloud formation greatly contributes wet deposition process. Using 2-dimensional cloud model, Flossmann[1] calculated deposition process of marine aerosols by cloud. Karamchandani and Venkatram[2] estimated formation process of surfeit in clouds by model. In this study, the developed long-range transport numerical model will be improved by following ways:

- adding in-cloud scavenging effects,
- increasing the resolution of meteorological model to evaluate clouds in the model,
- developing a method giving us results of high resolution while maintaining wide model area of the East Asia.

By this model, we will understand transport process of pollutants in long time period and estimate acid deposition over the East Asia.

2. Method

The model consists of two parts: one is a weather forecasting part which predicts meteorological variables, and the other is an advection-diffusion part of pollutants which uses meteorological variables forecasted by the former part as input data.

2-1. *Weather Forecasting Part*

This part of the model is almost the same as the routine weather forecasting model of the Japan Meteorological Agency (JMA). Details of this model are described in a technical report issued by the Numerical Prediction Division of JMA[3], [4]. Two meteorological models (finite difference limited area model over Asia region, and spectral limited area model around Japan) are nested to gain high resolution over focused area. The nesting method is the spectral nesting (Kida *et al.*[5]). The boundary values of the outer model is given by global analysis by JMA.

The primitive equations in σ-coordinates and the polar stereographic projection at 60°N are used in the model.

The calculation domain of the second model (Asian model) and the topography in the model are shown in Fig. 1.

The domain is covered horizontally by the Arakawa's B grid (73 x 55). The grid size is 127 km at 60°N. The inner-most model (Japan Spectral model) has a resolution of 40 km at 60°N. It has 19 layers in the vertical direction.

As the vertical eddy diffusion, we employ the closure model of level 2 (Mellor and Yamada[6]). At the lowest layer, Monin-Obukov's similarity theory is applied to

determine vertical fluxes from the lower boundary. The surface temperature is predicted.

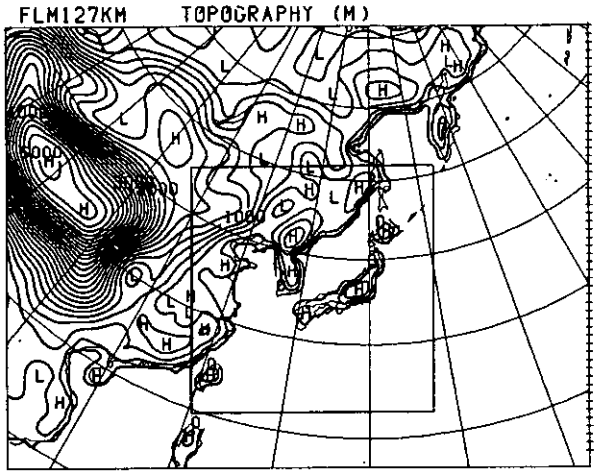

Fig. 1. Domain and the topography of the outer model. Inner frame indicates the area of the inner model.

We use two types of parameterization for precipitation process in the model: the large-scale condensation parameterization and the moist convective adjustment. The former prevents supersaturation and the latter keeps the atmospheric lapse rate between the dry adiabatic and the moist adiabatic lapse rate.

2-2. *Advection-Diffusion Part*

Advection and diffusion of pollutants are described by a random-walk model in the same coordinate systems as in the weather forecasting part. Winds, precipitation and diffusion coefficients used in the random walk model are predicted by the weather forecasting model. The variables are stored at every one hour integration of the forecast model.

The equations of the random walk model are:

$$\begin{cases} \dfrac{dX}{dt} = u \\ \dfrac{dY}{dt} = v \\ \dfrac{d\sigma}{dt} = \dot{\sigma} + R \end{cases},$$

where X, Y, and σ are positions of a particle in the three-dimensional space.
A random variable R is defined as

$$R = \pm\sqrt{\frac{2K_z}{\delta t}},$$

where K_z is the vertical diffusion coefficient derived from the forecast model, dt is the time interval in the random walk model, and the sign of the right-hand-side is chosen randomly for each particle and each time step.

A simplified Runge-Kutta method is employed for time integration of three-dimensional advection terms with a long time step dt = 10 min for the outer domain. We employ the Euler-backward scheme for random vertical diffusion terms with shorter time step dt = 2 min in order to avoid artificial convergence or divergence of particles at the layer where K_z varies abruptly. Each time step in the inner domain is decreased to 2/3 of the outer domain.

A particle is assumed to be deposited by a dry process if following two conditions are satisfied: the height of the particle is lower than a prescribed critical height H_{dep} = 0.99 in σ-coordinate, and a number given randomly for each particle and each time step is smaller than a value P_{ddep} defined as

$$P_{ddep} = \frac{V_{dep}\delta t}{H_{dep}},$$

where V_{dep} is the dry deposition velocity.

Wet deposition of the pollutants was estimated every one hour in the outer domain and 40 min in the inner domain. The particles are deposited on the surface with a probability of $P_{wdep} = C_{dep} \cdot dt \cdot RR$, where C_{dep} is the wet deposition rate, dt the estimated duration of wet deposition (one hour and 40 min in the respective domain) and RR is a precipitation factor.

The precipitation factor RR is defined as:

- for particles at grid points
  RR=1 if the predicted precipitation rate is greater than 0.05 mm/hour,
  RR=0 otherwise,
- for particles between grid points
  RR is interpolated horizontally using RRs around the particle.

3. Results

In order to verify the effect of the spectral nesting method on the calculation of long-range transport, a simulation is performed

in case of the Chernobyl nuclear power plant accident and the results are compared to the observation in Europe. As the observation data, the data distributed in the ATMES workshop[7] are used.

To examine the behavior of pollutants at the nesting boundary, the source of the pollutants is located in the outside of the inner model. Figure 2 shows simulated distribution of I^{131} in the air at 00 UTC on 1986.05.01., and indicates no significant problem around the nesting boundary.

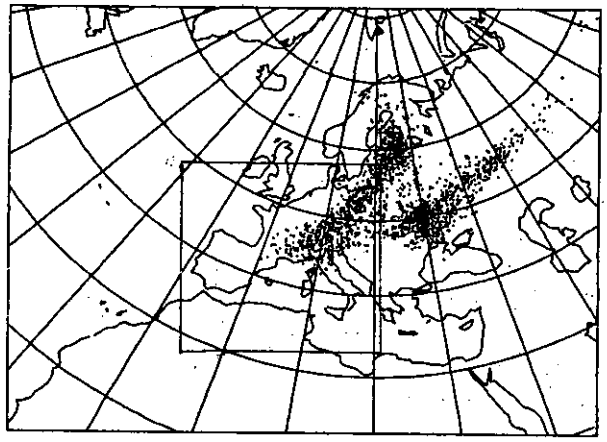

Fig. 2. Simulated distribution of I^{131} in the air at 00 UTC on 1986.05.01. Inner frame indicates the area of the inner model.

Next, we evaluate the nesting model statically by the following 4 cases:

- only the outer model is used, averaged concentration is calculated over 254×254 km (case 1),
- only the outer model is used, averaged concentration is calculated over 80×80 km (case 2),
- the inner model is nested, averaged concentration is calculated over 254×254 km (case 3),
- the inner model is nested, averaged concentration is calculated over 80×80 km (case 4).

The averaged time is 24 hours running mean. The results are shown in Table 1.

It is found in this table that nesting method is better than the non-nesting model both in RMSE and hit number. Comparing the different averaged areas, RMSE in the models with 80 km square averaging area are smaller than with the 254 km area, although hitting number in the models with 254 km square averaging area are larger with 80 km area. This indicates that narrower averaging area represents more locality and predicts better concentration of pollutants at the costs of increasing number of no-hit events.

Table 1. Root mean square error and number of hit, no-hit and false alarm of model for I^{131} over Europe.

Case	RMSE	Hit	No-hit	FA
1	0.994	348	129	4
2	0.874	277	203	1
3	0.905	397	76	8
4	0.818	314	165	2

References

1. Flossmann, A., *Tellus*, **42B**, 463-480 (1991).
2. Karamchandani, P. and A. Venkatram, *Atmos. Environ*, **26A**, 1041-1052 (1992).
3. Numerical Prediction Division, JMA, *Appendix to Periodic Rep. Num. Wea. Predict.*, 93 pp. (1986)
4. Numerical Prediction Division, JMA, *Explaining material of numerical prediction*, **20**, 55 pp. (1987).
5. Kida, H., T. Koide, H. Sasaki and M. Chiba, *J. Meteor. Soc. Japan*, **69**, 723-728 (1991).
6. Mellor, G. L. and T. Yamada, *J. Atmos. Sci.*, **31**, 1791-1807 (1974).
7. Satomura, T. and S. Yamada, *Tenki*, **39**, 71-73 (1992), (in Japanese).

A Study of Modeling of Local CO_2 Circulations

Contact Person: Laboratory Head, Yasuo Sato
Applied Meteorology Research Dept., Meteorological Research Institute,
1-1 Nagamine, Tsukuba, Ibaraki 305, Japan

Research Organization: Kazuo Mabuchi[1)],Hidetaka Sasaki,Takehiko Satomura,
Syunji Takahashi, Akira Yamamoto
Applied Meteorology Research Dept., Meteorological Research Institute,
Takashi Koide,Masaru Chiba,Kiyotaka Shibata
Climate Research Dept.,Meteorological Research Institute,
Takehisa Oikawa,Nobuko Saigusa
Department of Biology, University of Tsukuba
1) since 1 April 1994,Climate Research Dept.,MRI

Key Words: Carbon Cycle,Local Meteorology,CO2 Flux,Climate Model,
Surface Hydrology,Plant Physiological Process

1. Introduction

It is an especially important and basic issue to make clear the mechanism of carbon dioxide(CO2) circulations and budgets in the study of global warming. The CO2 missing sink issue shows that we have not had sufficient knowledge of CO2 circulations. Unless we can make clear the problem,it is difficult to predict the future image of the global warming phenomenon.

The CO2 circulations are deeply influenced by ecosystems, and especially through local weather and climate. Thus, we need to simulate CO2 circulations after modeling local weather and climate in a model study of CO2 circulations.

In this study,firstly we construct the model of the relation of local weather and surface hydrology prosseses including land ecosystems. Secondly,in the model, we numerically simulate daily variations of atmospheric CO2 concentration by estimating CO2 flux. As a result, we can estimate the atmospheric CO2 concentration. By doing so, it will be possible to evaluate the role of processes associated with CO2 missing sink and their relative degree of importance.

2. Method

Firstly,we develop a high-quality multi-nested local climate model. Secondly,we develop a simple surface hydrology model including plant physiological processes for use in a 3-dimensional local climate model. In that model,we treat explicitly CO2 fluxes between the atmosphere and land ecosystems according to daily variations of local weather. Thirdly, we simulate the local CO2 circulations and budgets with use of the developed model.

Lastly,through analyzing results of the model simulations,we investigate the role of variety of processes associated with CO2 missing sink, and their degree of relative importance.

3. Results.

We developed a 3-dimensional multi-nested local climate model to explicitly treat CO2 fluxes between the atmosphere and land ecosystems according to daily variations of local weather. The 4 models are nested. The most outside model is a global general circulation model. The second most outside model is the Fine-mesh Limited-area Model(FLM) and this model was nested to the Meteorological Research Institute(MRI) spectral General Circulation Model(GCM).